2. J. W. Black, W. A. M. Duncan, C. J. Durant, C. R. Ganellin, E. M. Parsons, *Nature* **236**, 385 (1972).
3. R. W. Brimblecombe *et al.*, *J. Int. Med. Res.* **3**, 86 (1975); R. Leth, B. Elander, U. Haglund, L. Olbe, E. Fellenius, *Am. J. Physiol.* **253**, G497 (1987).
4. D. E. Hernandez, G. A. Mason, C. H. Walker, J. E. Valenzuela, *Life Sci.* **41**, 2717 (1987); G. Glavin and A. Dugani, *ibid.*, p. 1397; G. B. Glavin, *J. Pharmacol. Exp. Ther.* **251**, 726 (1989); G. Gallagher, A. Brown, S. Szabó, *ibid.* **240**, 883 (1987); G. Glavin and S. Szabó, *Dig. Dis. Sci.* **35**, 1153 (1990); S. Szabó *et al.*, in *Advances in Dopamine Research*, M. Kohsaka, Ed. (Pergamon, New York, 1982), vol. 37, pp. 165–170; S. Szabó, *Lancet* ii, 880 (1979); _____ and C. H. Cho, *Toxicol. Pathol.* **16**, 205 (1988); S. Szabó *et al.*, *J. Pharmacol. Exp. Ther.* **240**, 871 (1987).
5. P. Sikiric *et al.*, *Dig. Dis. Sci.* **36**, 905 (1991).
6. T. Oishi and S. Szabó, *J. Pharmacol. Exp. Ther.* **240**, 879 (1987).
7. A. C. Guyton, *Textbook of Medical Physiology* (Saunders, Philadelphia, 1980).
8. Adult male Sprague-Dawley rats were used for these studies. They were decapitated, or anesthesized and subjected to transcardiac perfusion with fixative, and their stomachs and the upper portions of their duodenums were removed and frozen on dry ice. Twelve-micrometer-thick longitudinal sections were cut, and ISHH or immunostaining (or both) were performed. For ISHH alone, sections from ten rats were cut in a cryostat and thaw-mounted onto gelatin-coated slides. The slides were kept at −80°C until used. The procedure for ISHH was as described [W. S. Young III, E. Mezey, R. E. Siegel, *Mol. Brain Res.* 1, 231 (1986)]. Forty-eight nucleotide oligodeoxyribonucleotide probes were used. The probes were complementary to the mRNA nucleic acid sequences: H2: 645–692 and 936–983 [M. Ruat, E. Traiffort, J.-M. Arrang, R. Leurs, J.-C. Schwartz, *Biochem. Biophys. Res. Commun.* **179**, 1470 (1991)]; GR: 135–182 [A. S. Kopin *et al.*, *Proc. Natl. Acad. Sci. U.S.A.* **89**, 3605 (1992)]; D1: 810–857 [F. J. Monsma, L. C. Mahan, L. D. McVittie, C. R. Gerfen, D. R. Sibley, *ibid.* **87**, 6723 (1990)]; D2: 783–787 [J. R. Bunzow *et al.*, *Nature* **336**, 783 (1988)]; D3: 67–114 [P. Sokoloff, B. Giros, M.-P. Martres, M.-L. Bouthenet, J.-C. Schwartz, *ibid.* **347**, 146 (1990)]; D4: 733–774 and 829–882 [H. H. M. Van Tol *et al.*, *ibid.* **350**, 610 (1991)]; D5: 1–48 and 967–1011 [R. K. Sunahara *et al.*, *ibid.*, p. 614]; M1: 9–57 [T. I. Bonner, N. J. Buckley, A. C. Young, M. R. Brann, *Science* **237**, 527 (1987)]; M2: 255–303 [J. Gocayne *et al.*, *Proc. Natl. Acad. Sci. U.S.A.* **84**, 8296 (1987)]; M3: 6–51, M4: 9–57 [T. I. Bonner, N. J. Buckley, A. C. Young, M. R. Brann, *Science* **237**, 527 (1987)]; M5: 4–51 [T. I. Bonner, A. C. Young, M. R. Brann, N. J. Buckley, *Neuron* **1**, 403 (1988)]; TH: 1441–1488 [B. Grima, A. Lamouroux, F. Blanot, N. F. Biguet, J. Mallet, *Proc. Natl. Acad. Sci. U.S.A.* **82**, 617 (1985)]; DBH: 115–162 [A. Lamoroux *et al.*, *EMBO J.* **6**, 3921 (1987)]; and PNMT: 183–233 [E. Mezey, *Nucleic Acids Res.* **17**, 2125 (1989)]. The sections were coated with Kodak NTB3 emulsion and developed after 2 to 3 days (D3 to 5, M1 to 5, and TH) or 1 to 2 weeks (GR, D1, and D2). In all these cases, when two different oligonucleotides were used to probe the same mRNA, both probes showed the same pattern of labeling. In addition, sense strand probes based on the sequences of the D4 and D5 receptor mRNAs gave no cellular labeling.
9. E. Mezey and M. Palkovits, unpublished data.
10. S. Szabó and S. Reichlin, *Gastroenterology* **76**, 1257 (1979); S. Szabó, L. R. Haith, E. S. Reynolds, *Dig. Dis. Sci.* **24**, 471 (1979); S. Szabó and G. Pihan, *Chronobiol. Int.* **4**, 31 (1987).
11. G. B. Glavin *et al.*, *Brain Res. Rev.* **16**, 301 (1991).
12. E. Mezey and M. Palkovits, unpublished data.
13. J. Bienstock and A. D. Befus, *Immunology* **41**, 249 (1980); L. L. Brandborg, *Gastroenterology* **57**, 191 (1969); P. A. Crabbé, A. O. Carbonara, J. F. Heremans, *Lab. Invest.* **14**, 235 (1965); P. A. Crabbé and J. F. Heremans, *Gastroenterology* **51**, 305 (1966); C. Fiocchi, in *Immunology and Immunopathology of the Liver and Gastrointestinal Tract*, S. R. Targan and F. Shanahan, Eds. (Igaku-Shoin, New York, 1990), pp. 107–138; P. H. Guth and P. Hall, *Gastroenterology* **50**, 562 (1966); I. Roitt, *Essential Immunology* (Blackwell, London, 1988); T. Tomasi, *N. Engl. J. Med.* **279**, 1327 (1968).
14. For immunocytochemistry, three rats were anesthesized with ether and perfused through the ascending aorta with 300 ml of 4% paraformaldehyde and 1% picric acid in 0.1 M sodium phosphate buffer (pH 7.4). The stomachs were quickly removed, postfixed in the same fixative for 2 hours at 4°C, and soaked in a cryoprotectant solution [20% sucrose and 3% polyethylene glycol (400 MW) in physiological saline] overnight. The tissues were then frozen in isopentane at −80°C. Longitudinal 10-μm-thick sections were cut in a cryostat (Reichert-Jung Frigocut 2800E) and stored at −80°C until they were stained. Sections were immunostained and then processed for ISHH. The slides were first incubated with the primary antibody overnight at 4°C. The sections were then washed in 0.1 M phosphate-buffered saline (PBS) (pH 7.2) and transferred into a 1:100 dilution of an antibody to mouse IgG conjugated to fluorescein isothiocyanate (FITC) (Sigma) for 1 hour at room temperature. At the end of this incubation, the slides were transferred into PBS and the ISHH procedure was performed. The antibodies used to stain immunocytes included mouse monoclonal antibody to rat macrophage (1:400, Chemicon 1435, raised against peritoneal macrophages); antibody to rat mast cells conjugated to FITC (1:100, Accurate Chemicals); antibody to rat IgA conjugated to rhodamine or FITC (1:50, Nordic Immunology); antibody to rat IgE and antibody to rat IgM (1:400, Pierce); and antibody to rat IgG conjugated to phycoerythrin (1:100, Jackson Immunologicals). The secondary antibodies were antibody to mouse IgG or antibody to goat IgG conjugated to FITC or rhodamine (1:100, Sigma).
15. A. H. Soll, *J. Clin. Invest.* **61**, 370 (1978).
16. C. N. Chuang, M. C. Y. Chen, A. H. Soll, *Scand. J. Gastroenterol.* **26** (suppl. 180), 95 (1991).
17. A. H. Soll *et al.*, *Am. J. Physiol.* **247**, G715 (1984).
18. D. S. Bredt and S. H. Snyder, *Neuron* **8**, 3 (1992); C. J. Lowenstein and S. H. Snyder, *Cell* **70**, 705 (1992).
19. We thank Gy. Harta for the technical help and R. Dreyfuss for his help with photography.

22 May 1992; accepted 2 October 1992

Solution Structure of the SH3 Domain of Src and Identification of Its Ligand-Binding Site

Hongtao Yu, Michael K. Rosen, Tae Bum Shin, Cynthia Seidel-Dugan, Joan S. Brugge, Stuart L. Schreiber*

The Src homology 3 (SH3) region is a protein domain of 55 to 75 amino acids found in many cytoplasmic proteins, including those that participate in signal transduction pathways. The solution structure of the SH3 domain of the tyrosine kinase Src was determined by multidimensional nuclear magnetic resonance methods. The molecule is composed of two short three-stranded anti-parallel β sheets packed together at approximately right angles. Studies of the SH3 domain bound to proline-rich peptide ligands revealed a hydrophobic binding site on the surface of the protein that is lined with the side chains of conserved aromatic amino acids.

Mutational analysis of the Src protein kinase suggests that the SH3 domain of this protein, like the SH2 domain, may act as a regulatory element with dual functions—to modulate catalytic activity and to facilitate binding to other cellular proteins. Deletion or substitution of amino acids within the SH3 domain enhances the catalytic activity and oncogenic potential of Src (*1*), and prevents binding of at least one Src substrate (p110) (*2*). Similar results have been observed with the SH3 domain of the related protein tyrosine kinase, Abl (*3*, *4*), and a protein (3BP-1) has been identified that binds to the SH3 domains of Abl and Src in vitro (*5*). The 3BP-1 protein contains a sequence outside of its SH3 binding domain that is similar to the guanosine triphosphatase (GTPase) activation domain of several GTPase activating proteins (GAPs) that regulate the Rho/Rac family of guanine nucleotide binding proteins (*5*). Although the functional role of the SH3–3BP-1 interaction in vivo has not been established, certain SH3 domains appear to participate in signal transduction pathways that include both tyrosine kinases and small guanine nucleotide binding proteins (*6–9*). It is possible that these domains bind to GAPs and guanine nucleotide exchange factors (GEFs) that regulate the activity of guanine nucleotide binding proteins.

Neither the ligand specificities nor structures of SH3 domains have been determined. We report the structure determination of the SH3 domain of Src and the identification of its ligand binding site by multidimensional nuclear magnetic resonance (NMR) methods. The backbone fold and receptor site of Src SH3 are unrelated to those of the SH2 domains in Src, Abl, and the p85α subunit of phosphatidylinositol-3′ kinase (PI3′K) (*10*).

The sequential assignment of a 64-resi-

H. Yu, M. K. Rosen, T. B. Shin, S. L. Schreiber, Department of Chemistry, Harvard University, Cambridge, MA 02138.
C. Seidel-Dugan and J. S. Brugge, ARIAD Pharmaceuticals, Inc., Cambridge, MA 02139.
*To whom correspondence should be addressed.

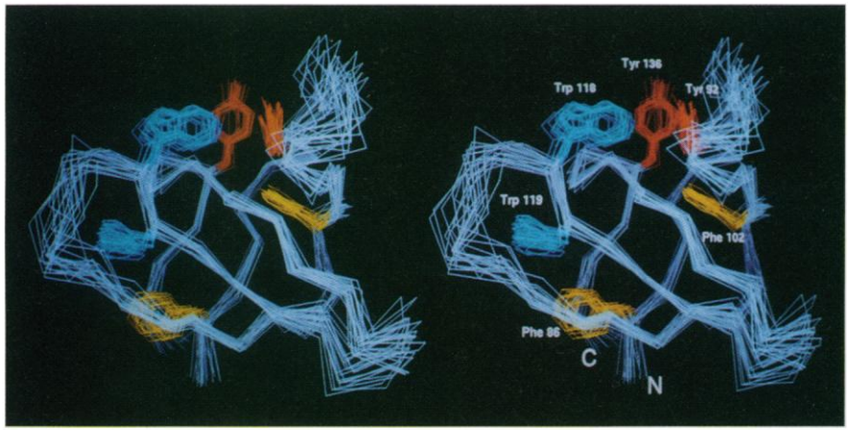

Fig. 1. Stereoview of overlay of 20 final refined structures of the Src SH3 domain (residues 85 to 140). The first eight residues of the SH3-containing peptide showed no NOEs to the remainder of the protein, and had relaxation rates and chemical shifts indicative of random structure. These residues were not included in structure calculations. The α-carbon trace and hydrophobic, aromatic side chains are shown. The side chain of Tyr^{90}, which lies behind that of Tyr^{92}, and the disordered surface side chain of Tyr^{131} were removed for clarity. The α-carbon traces are light blue, Tyr side chains are red, Phe side chains are yellow, and Trp side chains are dark blue. The proximal NH_2- and COOH-termini are located on the back sheet and are labeled N and C, respectively. The average RMSDs, calculated from the average coordinates, are 0.86 Å for the backbone atoms and 1.39 Å for all heavy atoms.

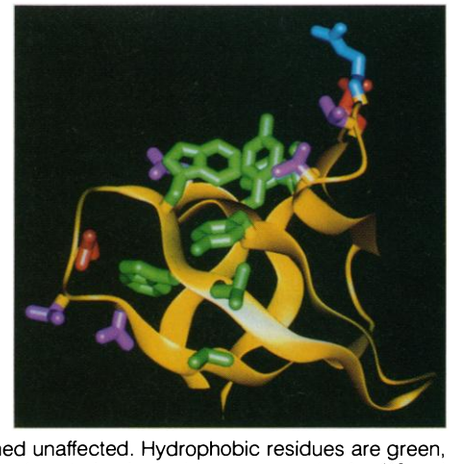

Fig. 2. Ribbon trace of the refined average Src SH3 structure depicting side chains of residues that show a change in their amide ^{15}N or ^{1}HN chemical shifts or both after the binding of the peptides PPPLPPLV and APTMPPPLPPGGK. The two peptides derived from 3BP-1 were synthesized on an ABI peptide synthesizer and purified by reverse phase high performance liquid chromatography. The SH3 binding peptide was added to the ^{15}N-labeled SH3 sample in a 1:1 ratio. ^{1}H-^{15}N HSQC spectra were taken of ^{15}N-SH3 before and after the addition of lyophilized peptide. Comparison of the two pairs of spectra shows that the amide ^{15}N or ^{1}H chemical shifts of residues Tyr^{92}, Arg^{95}, Thr^{96}, Thr^{98}, Val^{111}, Asn^{113}, Thr^{114}, Glu^{115}, Trp^{118}, Trp^{119}, Leu^{120}, Tyr^{131}, Asn^{135}, and Tyr^{136} changed by >0.1 ppm (^{1}H) or >0.5 ppm (^{15}N) upon peptide binding, whereas the others remained unaffected. Hydrophobic residues are green, acidic residues are red, basic residues are blue, and neutral polar residues are purple. Asn^{113} and Thr^{114}, shown in purple to the left, mark the site of the inserts discussed in the text.

due peptide containing the SH3 domain of Src [residues 85 to 140; the residue numbering system used throughout the text is that of full-length c-Src from chicken (*11*)] was done in a straightforward manner with three-dimensional ^{1}H total correlation ^{15}N-^{1}H heteronuclear multiple quantum coherence (TOCSY-HMQC) (*12*) and ^{1}H nuclear Overhauser enhancement ^{15}N-^{1}H HMQC (NOESY-HMQC) (*12, 13*) spectra in combination with two-dimensional ^{1}H double quantum filtered correlation spectroscopy (DQF-COSY) (*14*), Relay-COSY (*15*), and double quantum (DQ) (*16*) spectra recorded in H_2O (*17*). Structures were generated with a simulated annealing protocol that uses experimental distance and dihedral angle restraints (*18*). Derivation of experimental restraints is described in the legend to Table 1. A summary of the structural and geometrical statistics of the 20 final calculated structures is shown in Table 1. The average root-mean-square deviations (RMSDs) of the 20 calculated structures (residues 85 to 140) from the mean coordinate positions are 0.86 ± 0.17 Å for the backbone atoms and 1.39 ± 0.20 Å for all heavy atoms. Residues 93 to 99 and 112 to 117 are less well defined than the rest of the structure because of a lower density of long-range and medium-range NOEs. RMSD values excluding these regions are 0.68 ± 0.08 Å for the backbone atoms and 1.06 ± 0.09 Å for all heavy atoms. None of the structures have NOE violations over 0.3 Å or dihedral angle violations larger than 3°. The atomic coordinates of the 20 final structures will be deposited in the Brookhaven Protein Data Bank.

The SH3 domain structure consists of two three-stranded anti-parallel β sheets. The first sheet consists of residues 107 to 111, 118 to 124, and 129 to 132 (front in Fig. 1), and has a strong right-handed twist. The shorter second sheet contains residues 85 to 92, 99 to 102, and 137 to 140, and is packed against the first at approximately right angles. The interface of the sheets forms a hydrophobic core composed of residues Phe^{86}, Leu^{100}, Phe^{102}, Leu^{108}, Ile^{110}, Ile^{132}, and Val^{137}. Similar hydrophobic residues are found in analogous positions in other SH3 domains. The NH_2- and COOH-termini are located in adjacent strands at the ends of the second β sheet; their proximity allows the SH3 domain to exist as an independent entity in proteins with minimal disruption of the surrounding structure. A similar feature is also found in SH2 domains (*10*). The SH3 structure has two other identifiable elements of regular secondary structure—a type II β turn at residues 103 to 106 and a 3_{10} helix at residues 133 to 137 that consists of two consecutive type III β turns. The Src SH3 domain contains only three slowly exchanging amide protons, which suggests that the structure may be somewhat fluxional (*19*). This may not be a general feature of SH3 domains, however, because the SH3 domain from the p85α subunit of PI3′K has over thirty slowly exchanging amide protons under the same buffer conditions (*20*).

The ligand binding site was inferred from the identification of amino acid residues in the ^{15}N-labeled SH3 domain that underwent a change in their ^{15}N or ^{1}HN chemical shifts after the addition of either of two peptide ligands. The proline-rich peptides used in these studies, PPPLPPLV and APTMPPPLPPGGK, have sequences derived from a region of 3BP-1 that binds to the SH3 domains of Abl and Src (*5*); mutagenesis has localized the Abl SH3 binding to a ten-residue proline-rich region in 3BP-1 (*21*). The ligand-induced perturbations were nearly identical for the two peptides, indicating that the PPPLPP sequence may specifically interact with the SH3 domain. The perturbed residues define a slightly curved, hydrophobic depression on the surface of the protein that is lined with side chains of aromatic amino acids (Fig. 2). Residues with ligand-induced changes in chemical shift are known to define a larger region of a protein than the actual receptor-ligand interface (*22*). Thus, the length of the SH3 binding site is slightly longer than the approximated length of an extended (trans-proline) conformation of the hexapeptide ligand.

Table 1. Structural and energetic statistics for the SH3 domain of Src. Three-dimensional structures were calculated from the experimental restraints with the program X-PLOR 2.0, by the reported protocol (*18, 27*). The generated structures were refined with the simulated annealing refinement protocol described in XPLOR 3.0 with minor modifications (*18*). The protocol contains a slow-cooling stage with the starting temperature at 2000K followed by 1000 steps of conjugate gradient energy minimization. The final concentration of the SH3 NMR sample was 3.5 mM SH3 in a solution containing 90% H_2O, 10% D_2O, 100 mM phosphate (pH 6.0), and 100 mM NaCl. The SA_i column gives the average and standard deviations for the indicated variables obtained from the 20 final refined simulated annealing structures. $\langle SA \rangle_{ref}$ represents the average structure of SA_i least-square fit to each other including all atoms and refined with 500 steps of steepest-descent energy minimization with the simulated annealing parameters. Distance and angular RMSDs are from the upper or lower bounds of the distance and angular restraints, respectively. NOE-based interproton distance restraints were derived from two-dimensional NOESY and three dimensional NOESY-HMQC spectra. Cross-peak intensities measured in 50 ms NOESY spectra were used to calibrate distance restraints based on known distances in regular secondary structural elements. Restraints were divided into three categories: weak (≤5.0 Å), medium (≤3.3 Å for NOEs involving only aliphatic protons, ≤3.5 Å for NOEs involving amide protons), and strong (≤2.7 Å); 0.5 Å was added to the upper limits for restraints involving methyl protons. Ambiguities in assignment of long-range NOEs involving methyl protons were to some extent resolved by an SH3 sample that was biosynthetically deuterated at the methyl protons of valine and isoleucine (*28*). We used 28 side chain χ_1 and 30 backbone ϕ angle restraints; these are based on coupling constants and cross-peak magnitudes measured in a double quantum filtered COSY spectrum and on intraresidue NOE data. In all cases, χ_1 values were restricted to a ±60° range, allowing stereospecific assignment of side chain protons based on NOEs from NH and CαH. The set of structural restraints was built in an iterative manner from initial structures generated with only a subset of the total restraints.

Parameter		SA_i	$\langle SA \rangle_{ref}$
RMSDs from experimental restraints			
RMS distance deviations (Å)			
All	(582)	0.017 ± 0.003	0.018
Interproton distances			
Intraresidue	(202)	0.011 ± 0.004	0.012
Interresidue sequential ($\|i - j\| = 1$)	(172)	0.017 ± 0.004	0.024
Interresidue short-range ($1 < \|i - j\| \leq 5$)	(32)	0.017 ± 0.006	0.010
Interresidue long-range ($\|i - j\| > 5$)	(164)	0.016 ± 0.005	0.014
Hydrogen-bond Restraints*	(12)	0.021 ± 0.009	0.014
RMS dihedral deviations (degrees)			
All	(58)	0.171 ± 0.052	0.085
Deviations from idealized geometry†			
Bonds (Å)	(888)	0.005 ± 0.000	0.005
Angles (degrees)	(1585)	1.658 ± 0.005	1.656
Impropers (degrees)	(428)	0.239 ± 0.031	0.231
Energetic statistics (kcal mol^{-1})			
E_{repel}‡		7.3 ± 1.5	5.2
E_{vdW}§		−91.7 ± 18.7	−98.8
E_{NOE}¶		8.5 ± 2.5	9.9

*Twelve distance restraints were included for six hydrogen bonds derived from three slowly exchanging amide protons and from three hydrogen bonds that are conserved in all the calculated structures and located at the center of the β sheet. †Idealized geometries based on CHARMM 19 parameters (*29*). ‡The value of the quartic repulsive force constant used in the structure calculations was 4 kcal mol^{-1} Å^{-4}. §Calculated with standard CHARMM 19 parameters (*29*). ¶The values of the square-well NOE and torsion angle force constants were 50 kcal mol^{-1} Å^{-2} and 200 kcal mol^{-1} rad^{-2}, respectively.

Many of the conserved amino acid residues in SH3 domains are found to be either directly associated with the ligand binding site or in close proximity to it; these amino acids may maintain the structure of the site. The sequence ALYDY (Src residues 88 to 92), which is the most characteristic feature of SH3 domains, defines one end of the receptor site (Figs. 1 and 2). Leu^{89} is found on a β-bulge, packed against Tyr^{90}. Another conserved aromatic amino acid, Tyr^{136}, also contacts the side chains of Tyr^{90} and Tyr^{92} and lines the receptor site. A somewhat less conserved sequence, Src residues Trp^{118} and Trp^{119}, is located further away from Tyr^{90} and Tyr^{92}. The side chain of Trp^{119} makes a number of contacts with hydrophobic residues in a loop that is expected to be of variable size in SH3 domains. The side chain of the more highly conserved Trp^{118} is oriented along the floor of the receptor site. Because the peptide ligands induce a change in chemical shift in each of the aforementioned aromatic amino acids, it is possible that they all take part in ligand binding. The other end of the binding site is defined by the loop containing Asn^{113} and Thr^{114} (Fig. 2). This would be the location of the insert of six amino acids that is found in a form of Src specific to neuronal cells (*23*), and of a longer insert inferred from a cDNA encoding a putative second form of neuronal Src (*24*). The structure suggests a basis for the observation that the neuronal Src SH3 domain displays weaker interactions with binding proteins than its non-neuronal variant (*5, 25*). It is likely that the insert will interfere with contacts normally made to the bound peptide at this end of the binding site. We anticipate that this same site corresponds to an insert in the larger (~75–amino acid) SH3 domain of the p85α subunit of PI3′K (*26*).

Although several residues in the ligand binding site are highly conserved among the different SH3 domains, there are many amino acids in the site that show little conservation (*26*). As it seems likely that all SH3 domains will adopt a similar three-dimensional structure, this lack of conservation implies that their binding specificities may be highly variable. Therefore, different SH3 domains may interact with distinct peptide motifs and thus mediate specific protein-protein interactions.

REFERENCES AND NOTES

1. J.-Y. Kato *et al.*, *Mol. Cell Biol.* **6**, 4155 (1986); W. M. Potts, A. B. Reynolds, T. J. Lansing, J. T. Parsons, *Oncogene Res.* **3**, 343 (1988); S. P. Nemuth, L. C. Fox, M. DeMarco, J. S. Brugge, *Mol. Cell. Biol.* **9**, 1109 (1989); C. Seidel-Dugan, B. E. Meyer, S. M. Thomas, J. S. Brugge, *ibid.* **12**, 1835 (1992).
2. S. B. Kanner, A. B. Reynolds, H.-C. R. Wang, R. R. Vines, J. T. Parsons, *EMBO J.* **10**, 1689 (1991).
3. P. Jackson and D. Baltimore, *ibid.* **8**, 449 (1989).
4. A. M. Pendergast *et al.*, *Proc. Natl. Acad. Sci. U.S.A.* **88**, 5927 (1991).
5. P. Cicchetti, B. J. Mayer, G. Thiel, D. Baltimore, *Science* **257**, 803 (1992).
6. J. Chenevert, K. Corrado, A. Bender, J. Pringle, I. Herskowitz, *Nature* **356**, 77 (1992).
7. J. Chant, K. Corrado, J. R. Pringle, I. Herskowitz, *Cell* **65**, 1213 (1991); D. Drubin, *ibid.*, p. 1093.
8. S. G. Clark, M. J. Stern, H. R. Horvitz, *Nature* **356**, 340 (1992).
9. A. Musacchio, T. Gibson, V.-P. Lehto, M. Saraste, *FEBS Lett.* **307**, 55 (1992).
10. G. W. Booker *et al.*, *Nature* **358**, 684 (1992); G. Waksman *et al.*, *ibid.*, p. 646; M. Overduin, C. B. Rios, B. J. Mayer, D. Baltimore, D. Cowburn, *Cell* **70**, 697 (1992).
11. The sequence of residues 85 to 140 is: TFVALYDYESRTETDLSFKKGERLQIVNNTEGDWWLAHSLTTGQTGYIPSNYVAPS. Protein samples used in these studies were prepared as follows: a cDNA encoding the Src SH3 domain (residues 81 to 140) was subcloned into the pGEX-2T vector (Pharmacia). Expression of the construct in *E. coli* yielded a glutathione-S-transferase–SH3 fusion protein. The fusion protein was purified on a glutathione-agarose affinity column and cleaved with digestion by thrombin. The cleavage mixture was purified by gel filtration chromatography. This procedure resulted in a protein with four NH_2-terminal residues (GSHM) derived from the construct, followed by residues 81 to 140 of chicken c-Src. The four GST and first four Src residues (GGVT) were not included in the structure calculations (see Fig. 1). The uniformly ^{15}N-labeled SH3 domain was obtained by growing the cells in M9 minimal medium containing $^{15}NH_4Cl$ as the sole nitrogen source. A selectively deuterated protein sample was obtained by growing the cells in M9 minimal medium supplemented with uniformly deuterated mixture of algal amino acids (400 mg/l). Before induction, 200 mg/l of tryptophan, phenylalanine, and leucine were added along with an additional 500 mg/l of deuterated algal amino acids. Purification of ^{15}N-labeled and selectively deuterated samples was as described above. Abbreviations for the amino acid residues

are: A, Ala; C, Cys; D, Asp; E, Glu; F, Phe; G, Gly; H, His; I, Ile; K, Lys; L, Leu; M, Met; N, Asn; P, Pro; Q, Gln; R, Arg; S, Ser; T, Thr; V, Val; W, Trp; and Y, Tyr.
12. D. Marion *et al.*, *Biochemistry* **28**, 6150 (1989).
13. S. W. Fesik and E. R. P. Zuiderweg, *J. Magn. Reson.* **78**, 588 (1988); D. Marion, L. E. Kay, S. W. Sparks, D. A. Torchia, A. Bax, *J. Am. Chem. Soc.* **111**, 1515 (1989); E. R. P. Zuiderweg and S. W. Fesik, *Biochemistry* **28**, 2387 (1989).
14. U. Piantini, O. W. Sørensen, R. R. Ernst, *J. Am. Chem. Soc.* **104**, 6800 (1982); A. J. Shaka and R. Freeman, *J. Magn. Reson.* **51**, 169 (1983); N. Müller, R. R. Ernst, K. Wüthrich, *J. Am. Chem. Soc.* **108**, 6482 (1986).
15. G. Eich, G. Bodenhausen, R. R. Ernst, *J. Am. Chem. Soc.* **104**, 3731 (1982); P. H. Bolton and G. Bodenhausen, *Chem. Phys. Lett.* **89**, 139 (1982); P. H. Bolton, *J. Magn. Reson.* **48**, 336 (1982); G. Wagner, *ibid.* **55**, 151 (1983).
16. A. Bax, R. Freeman, T. A. Frenkiel, M. H. Levitt, *J. Magn. Reson.* **43**, 478 (1981); G. Wagner and E. R. P. Zuiderweg, *Biochem. Biophys. Res. Comm.* **113**, 854 (1983).
17. A complete listing of ^{1}H and ^{15}N chemical shifts will be provided upon request by the authors.
18. A. T. Brünger, *X-PLOR Manual* (Yale University, New Haven, CT, 1988); *X-PLOR Manual V. 3.0* (Yale University, New Haven, CT, 1992).
19. Y. Patterson, S. W. Englander, H. Roder, *Science* **249**, 755 (1990).
20. S. Koyama, H. Yu, D. C. Dalgarno, S. L. Schreiber, unpublished results.
21. B. J. Mayer and D. Baltimore, personal communication.
22. C. Spitzfaden *et al.*, *FEBS Lett.* **300**, 291 (1992).
23. J. B. Levy, T. Dorai, L. H. Wang, J. S. Brugge, *Mol. Cell. Biol.* 7, 4142 (1987); R. Martinez, B. Mathey-Prevot, A. Bernards, D. Baltimore, *Science* **237**, 411 (1987).
24. J. M. Pyper and J. B. Bolen, *Mol. Cell. Biol.* **19**, 2035 (1990).
25. Z. Weng, J. A. Taylor, J. S. Brugge, C. Seidel-Dugan, in preparation.
26. M. Otsu *et al.*, *Cell* **65**, 91 (1991).
27. S. W. Michnick, M. K. Rosen, T. J. Wandless, M. Karplus, S. L. Schreiber, *Science* **252**, 836 (1991).
28. C. H. Arrowsmith, R. Pachter, R. B. Altman, S. B. Iyer, O. Jardetzky, *Biochemistry* **29**, 6332 (1990).
29. B. R. Brooks *et al.*, *J. Comput. Chem.* **4**, 187 (1983).
30. We thank A. Tanaka for preparing the peptide ligands used in these studies, D. C. Dalgarno for assisting in the acquisition of several NMR data sets, and Bruker Instruments for providing instrument time. Supported by fellowships from the American Chemical Society and Merck Sharp & Dohme Research Laboratories (M.K.R.) and from the Natural Sciences and Engineering Research Council of Canada (T.B.S.) and by grants from the National Cancer Institute (CA27951, J.S.B.) and the National Institute of General Medical Sciences (GM44993, S.L.S.). The NMR facilities at the Harvard University Department of Chemistry Instrumentation Center were supported by the NIH (grant I-S10-RR04870) and NSF (grant CHE88-14019).

1 October 1992; accepted 6 November 1992

Behavioral Lifetime of Human Auditory Sensory Memory Predicted by Physiological Measures

Z.-L. Lu, S. J. Williamson,* L. Kaufman

Noninvasive magnetoencephalography makes it possible to identify the cortical area in the human brain whose activity reflects the decay of passive sensory storage of information about auditory stimuli (echoic memory). The lifetime for decay of the neuronal activation trace in primary auditory cortex was found to predict the psychophysically determined duration of memory for the loudness of a tone. Although memory for the loudness of a specific tone is lost, the remembered loudness decays toward the global mean of all of the loudnesses to which a subject is exposed in a series of trials.

Stimulation of human sense organs is initially represented for a brief period by a literal, labile, and modality-specific neural copy. The term iconic memory refers to the initial representation of visual stimuli, and echoic memory is its counterpart for auditory stimulation (*1*). The latter form of memory is essential for integration of acoustic information presented sequentially over an appreciable period of time (*2*). Memory experiments suggest that the duration of echoic memory is about 2 to 5 s (*3*). We lack physiological evidence for the locus of echoic memory, although psychophysical experiments (*4*) suggest a central rather than peripheral site for memory storage.

The nature of decay of sensory memory is by no means clear. The simple decay of sensory memory could be reflected by an increase in uncertainty of the comparison of recently heard memory items with a probe item. However, even this approach might be constrained by the possibility that subjects retain general information about the context but lose information about the specific item. Early in this century, Hollingworth (*5*) discovered a central tendency: The judged magnitude of a stimulus (measured in different modalities) lies near the middle of the range of stimuli used in the experiment (*6*). The range of stimuli also affects subsequent judgments of these stimuli (*7*). Experiments using the method of partial report (*8*) suggest that the decay of sensory memory is a passive process, so that it may well be reflected in reproducible characteristics of neuronal activity.

Z.-L. Lu and S. J. Williamson, Department of Physics and Center for Neural Science, New York University, New York, NY 10003.
L. Kaufman, Department of Psychology and Center for Neural Science, New York University, New York, NY 10003.

*To whom correspondence should be addressed.

Experiments with animals (*9*) indicate the presence of a neuronal memory trace by a decrement in the responses of single cells when a stimulus is presented repetitively. Advances in magnetoencephalography (MEG) have made it possible to determine noninvasively the strength of neuronal activity in specific sensory regions in the human brain with high sensitivity and temporal resolution (*10*). This technique revealed that the neuronal activation trace in primary auditory cortex established 100 ms after the onset of a tone stimulus (the N100 component) decays exponentially with time. This approach also showed that the lifetime in association cortex is several seconds longer than that in primary cortex (*11*). These findings confirm the idea that short-term memory traces are modality-specific (*12*). Further, the results show that the N100 component of the event-related potential or field may well play a role in echoic memory, although no evidence was found for this component that supports short-term memory scanning (working memory) (*13*).

Four right-handed adults (two males and two females) volunteered as subjects after providing informed consent (*14*). The task for each subject was a two-alternative forced choice: press one button if the probe tone appeared louder than the test tone or the other button if it appeared softer (*15*). No immediate feedback was provided, but subjects were informed of the experimental results after the end of each session. A total of 6000 trials was collected for each subject. All the analyses were based on the data after exclusion of the first 20% of the trials of every session. We discounted these results because it was during this first set of presentations that the range of the loudness in the session was established. For each delay condition, a cumulative Gaussian distribution was fit to the psychophysical data of loudness judgments. The equal loudness point was defined as the mean of the Gaussian distribution, and the uncertainty was the standard deviation of the distribution. Separate magnetic field recordings of auditory-evoked responses of similar tones were also collected for the subjects for whom there were no existing MEG data (*11*).

Figure 1 illustrates the neuromagnetic data with which the psychophysical data were compared. The strength of the N100 component of the response of primary auditory cortex increased with the interstimulus interval (ISI) and approached a maximum value for ISIs exceeding a few seconds. In all cases, such curves could be fit by the mathematical expression $A(1 - e^{-(t-t_0)/\tau})$, with fitting parameters of amplitude A, lifetime τ, and time of decay onset t_0 (*16*). We emphasize that the shape of the curve in each case is determined by a single